Resolvent Analysis: With or Without Eddy Viscosity?

P Morra, O Semeraro, D S Henningson, Carlo Cossu

Resolvent Analysis: With or Without Eddy Viscosity?

P. Morra[1], O. Semeraro[2], D. S. Henningson[1] and C. Cossu[3]

[1] *KTH Royal Institute of Technology, Linné FLOW Centre, Dept. of Mechanics, SE-10044, Stockholm, Sweden*
[2] *LIMSI, UPR 3251 CNRS / Université Paris-Saclay, 91400 Orsay, France*
[3] *LHEEA, UMR 6598 CNRS / Centrale Nantes, 44300 Nantes, France*

Abstract

In this study, estimations of the spatio-temporal power cross-spectral density based on the resolvent operator are compared to those obtained by direct numerical simulation (DNS) in the turbulent plane channel flow at $Re_\tau = 1007$ by analysing separately the contribution of each temporal frequency ω. The comparison is performed for spatial scales characteristic of buffer-layer and large-scale motions. Good agreement between the resolvent-based estimates and the statistics obtained by DNS is found when the resolvent operator is based on a linear model which includes the effect of an eddy-viscosity modelling the effect of turbulent Reynolds stresses. The agreement is further improved when a colored noise matching the measures is used instead of white noise in the forcing modelling. Such a good agreement is not observed when the eddy-viscosity terms are not included in the linear model. In this case, the estimation based on the resolvent is unable to select the right peak frequency and wall-normal location of buffer-layer motions.

1 Introduction

Coherent streamwise streaks, i.e. spanwise alternated high- and low-velocity regions elongated in the streamwise direction, account for most of the fluctuating energy in wall-bounded turbulent shear flows. Their ubiquity in transitional and turbulent flows has been related to the 'lift-up' effect where low-energy quasi-streamwise vortices immersed in a shear flow lead to high-energy streamwise streaks. Much attention has been given to the computation of optimal energy amplifications associated to the lift-up effect and of the associated optimal inputs and outputs for the linear initial-value problem and the response to harmonic and stochastic forcing.

In the case of turbulent flows, two distinct approaches have been followed to the definition of the linear operator used for the computation of optimal energy amplifications. In the first approach the Navier-Stokes equations are rewritten in terms of perturbations to the turbulent mean velocity; the instantaneous and averaged (Reynolds stresses) perturbation nonlinear terms are accounted for as an external input which forces the response via the linear operator (see e.g. [1, 2, 3, 4] among others and [5] for a review). In the second approach the 'incoherent' part of turbulent Reynolds stresses is included in the linear operator with an eddy-viscosity (ν_t) model (see [6, 7, 8, 9, 10, 11, 12, 13] among others and [14] for a review). We will refer to the former approach as 'ν-model' and to the latter as 'ν_t-model'.

Most of the comparisons between statistics of real turbulent flows and the predictions based on the two mentioned linear models, and in particular those where the resolvent modes are computed, are, however, either qualitative or concern integrated energy densities and (integrated) spatial spectra (the Fourier transform of the second-order velocity spatial correlations). Also, most of these analyses, with the notable exception of [15], lack a detailed quantitative comparison of the performance of the ν and ν_t models.

A major source of difficulty for the comparison of turbulent statistics to predictions of linear models resides in the presence of a wide range of temporal frequencies involved in turbulent processes, even at selected spatial scales which can not be separated when considering spatial correlations tensors. In the context of Karhunen-Loève decompositions (proper orthogonal decompositions, POD) the use of the *spatio-temporal* correlation tensor $\mathbf{R}(\mathbf{x}, \mathbf{x}+\Delta\mathbf{x}, t, t+\tau)$ and of its Fourier-transform where the effect of different frequencies can be separated has led a direct connection between the spectral-POD modes and resolvent modes (see e.g. [16, 17, 18]) based on the ν-model.

The scope of this investigation is, inspired by this recent progress, to evaluate the respective performance of the ν-model and the ν_t-model in the estimation of the velocity *spatio-temporal* power spectral density and power cross-spectral density. The turbulent channel flow at $Re_\tau = 1007$ is used as a testbed for this analysis because of the large inhomogeneity of ν_t in this flow which enhances potential differences of the two models.

2 Background

We consider the dynamics of coherent perturbations in a turbulent flow of an incompressible fluid of kinematic viscosity ν in the channl between two infinite parallel walls located at $y = \pm h$. We denote the streamwise, wall-normal and spanwise coordinates by x, y and z, respectively.

In the 'ν_t-model', the evolution of small coherent perturbations to the turbulent mean flow is modelled with linearised equations which include the effect of the turbulent Reynolds stresses by means of an eddy viscosity ν_t corresponding to the turbulent mean flow profile $\mathbf{U} = (U(y), 0, 0)$ [6, 7, 9, 11]. Considering dimensionless variables based on the reference length h and the reference velocity $(3/2)U_{bulk}$, where U_{bulk} is the constant mass-averaged streamwise velocity, this model reads:

$$\frac{\partial \mathbf{u}}{\partial t} + \nabla\mathbf{u}\cdot\mathbf{U} + \nabla\mathbf{U}\cdot\mathbf{u} = -\nabla p + \nabla\cdot\left[\nu_T\left(\nabla\mathbf{u} + \nabla\mathbf{u}^T\right)\right] + \mathbf{f}, \tag{1}$$

where $\mathbf{u} = (u, v, w)$ and p are the coherent perturbation velocity and pressure, $\nu_T(y) = \nu + \nu_t(y)$ is the total effective viscosity and $\mathbf{f}$ is the forcing term (note that in dimensionless units $\nu_T = (1 + \nu_t/\nu)/Re$, where $Re = (3/2)U_{bulk}h/\nu$). The incompressibility condition $\nabla\cdot\mathbf{u} = 0$ completes these equations. The eddy viscosity

is modelled with the semi-empirical expression proposed by Cess [19], as reported in [6]:

$$\frac{\nu_t}{\nu} = \frac{1}{2}\Big\{1+\frac{\kappa^2 {Re_\tau}^2}{9}(1-y^2)^2(1+2y^2)^2(1-e^{y^+/A})^2\Big\}^{1/2}-\frac{1}{2}, \quad (2)$$

where $y \in [-1,1]$, $y^+ = Re_\tau(1-|y|)$ and $Re_\tau = u_\tau h/\nu$ is the Reynolds number based on the friction velocity u_τ. The von Kármán constant is set to $\kappa = 0.426$ and the constant $A = 25.4$ as in [11, 13].

In the 'ν-model' (a.k.a. 'quasi-laminar model'), turbulent Reynolds stresses and nonlinear terms are both included in the forcing term $\mathbf{f}$ so that the linear model reduces to Eq. (1) but now only including the molecular kinematic viscosity $\nu_T = \nu$ [2, 20, 4].

The system invariance to translations in wall-parallel directions leads to consider the Fourier-modes $\hat{\mathbf{u}}(\alpha,y,\beta,t)e^{i(\alpha x+\beta z)}$ and $\hat{\mathbf{f}}(\alpha,y,\beta,t)e^{i(\alpha x+\beta z)}$ of streamwise and spanwise wavenumbers $\alpha = 2\pi/\lambda_x$ and $\beta = 2\pi/\lambda_z$. Eq. (1) can be reduced to the following linear system, expressed in terms of the state vector $\hat{\mathbf{q}} = [\hat{v},\hat{\omega}_y]^T$ formed with the wall-normal components of the velocity and vorticity Fourier modes:

$$\frac{\partial \hat{\mathbf{q}}}{\partial t} = \mathbf{A}\hat{\mathbf{q}} + \mathbf{B}\hat{\mathbf{f}}, \quad (3)$$

where $\hat{\mathbf{u}} = \mathbf{C}\hat{\mathbf{q}}$ and $\hat{\mathbf{q}} = \mathbf{D}\hat{\mathbf{u}}$ (the explicit expressions of the operators $\mathbf{A}$, $\mathbf{B}$, $\mathbf{C}$ and $\mathbf{D}$ can be found e.g. in [13]). As the system is linearly stable, the response to deterministic can be analysed in the frequency domain considering the harmonic forcing $\hat{\mathbf{f}} = \widetilde{\mathbf{f}}e^{-i\omega t}$ with the harmonic response $\widetilde{\mathbf{u}}e^{-i\omega t}$ related by:

$$\widetilde{\mathbf{u}} \;=\; \mathbf{H}\widetilde{\mathbf{f}} \quad ; \quad \mathbf{H} = -\mathbf{C}(i\omega\mathbf{I}+\mathbf{A})^{-1}\mathbf{B} \quad (4)$$

where $\mathbf{H}$ is the resolvent operator (or transfer function). When the forcing is stochastic so is the response and one has to consider velocity second-order *spatio-temporal* correlation tensor

$$\mathbf{R}(\xi,y,y',\zeta,\tau) = \langle \mathbf{u}(x,y,z,t)\mathbf{u}^*(x+\xi,y',z+\zeta,t+\tau)\rangle, \quad (5)$$

where $\langle\ \rangle$ denotes ensemble averaging and * denotes complex conjugate transpose. The (spatio-temporal) power cross-spectral density tensor $\mathbf{S}(\alpha,y,y',\beta,\omega)$ is obtained through Fourier transform of $\mathbf{R}$ in ξ, ζ and τ.

The tensor $\mathbf{S}$ can also be obtained directly as the average of the Fourier transform $\widetilde{\mathbf{u}}$ of the velocity [21] and the stochastic forcing power cross-spectral density tensor $\mathbf{P}$ can be defined similarly:

$$\mathbf{S}(\alpha,y,y',\beta,\omega) = \langle \widetilde{\mathbf{u}}(\alpha,y,\beta,\omega)\widetilde{\mathbf{u}}^*(\alpha,y',\beta,\omega)\rangle \quad (6)$$

$$\mathbf{P}(\alpha,y,y',\beta,\omega) = \langle \widetilde{\mathbf{f}}(\alpha,y,\beta,\omega)\widetilde{\mathbf{f}}^*(\alpha,y',\beta,\omega)\rangle. \quad (7)$$

An estimation $\mathbf{S}^{(est)} = \mathbf{HPH}^*$ of the velocity power cross-spectral density tensor is obtained by replacing the linear expression of Eq. (4) in Eq. (7). Further assuming that $\mathbf{P} = p(\alpha,\beta,\omega)\,\mathbf{I}$ (where $\mathbf{I}$ is the identity operator), as e.g. in [3, 12, 13], then $\mathbf{S}^{(est)}$ reduces to:

$$\mathbf{S}^{(res)} = p\mathbf{H}\mathbf{H}^* \quad (8)$$

which is the basic expression used in resolvent analyses. The scope of this study is to determined the accuracy of the estimation provided by Eq. (8).

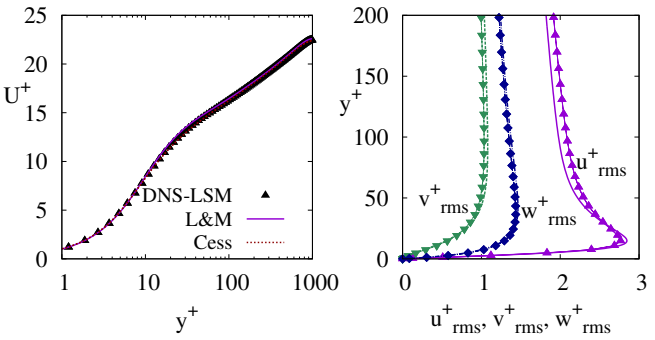

Figure 1: Comparison of direct numerical simulations in the LSM flow unit (DNS-LSM) at $Re_\tau = 1007$ to those in [22] (L&M) and to Cess's model at $Re_\tau = 1000$ in terms of mean flow profiles (left panel) and *rms* velocity profiles (right panel) from the DNS-LSM (lines with symbols) compared to those of L&M (lines)

3 Direct numerical simulation and statistics

The velocity correlations have been estimated trough a direct numerical simulation of the turbulent channel flow at $Re_\tau = 1007$ in a domain of extension $L_x = 3$ and $L_z = 1.5$ corresponding to the size of the most energetic large-scale motions (LSM) in the channel [23] and representing the minimum flow unit for the self-sustainment of coherent LSM [24].

The simulations have been performed using the pseudospectral `SIMSON` code which uses Fourier expansions in the streamwise and spanwise directions, where periodicity is enforced, and Chebyshev expansions in the wall-normal direction to solve the three-dimensional time-dependent incompressible Navier-Stokes equations in the channel [25]. A total of $N_x = 128, N_y = 129, N_z = 128$ points have been used with a uniformly spaced grid in x and z and Gauss-Lobatto points in y. This corresponds to a grid spacing $\Delta x^+ = 23, \Delta z^+ = 12$ and to $\Delta y^+_{min} = 0.3$ near the wall and $\Delta y^+_{max} = 24$ at the channel centre. This chosen grid is coarser than those typically used in DNS at this Reynolds number to keep the data analysis manageable.

As shown in Figure (1), despite the moderate extension of the domain and the relatively coarse grid, the computed mean flow and the *rms* fluctuation profiles are in reasonable agreement with those of [22] obtained in the much larger domain $L_x = 25, L_z = 9.5$ with a finer grid ($\Delta x^+ = 11, \Delta z^+ = 5$) We have further verified Cess's analytic fit by comparing the mean flow profile and the corresponding eddy viscosity to the ones issued by DNS data.

The analysis of the premultiplied streamwise kinetic energy spectral density $\alpha\beta E_{uu}(\alpha,y,\beta) = \alpha\beta\int_{-\infty}^{\infty} S_{uu}(\alpha,y,y,\beta,\omega)d\omega$, evaluated in the $y^+ = 15$ and $y = 0.5$ planes (not shown here) shows that the most energetic structures at $y = 0.5$ have spatial scales corresponding to the dimensions of the LSM flow unit $\lambda_x = L_x = 3$, $\lambda_z = L_z = 1.5$ (corresponding to $\alpha \approx 2$, $\beta \approx 4$) while the most energetic structures at $y^+ = 15$ have spatial scales $\lambda_x^+ \approx 450$ and $\lambda_z^+ \approx 100$ (corresponding to $\alpha \approx 14$, $\beta \approx 63$ at $Re_\tau = 1007$) typical of the near-wall self-sustained process. We will therefore focus on these two sets of (α,β), corresponding to $(\lambda_x = 3, \lambda_z = 1.5)$ and $(\lambda_x^+ = 450, \lambda_z^+ = 100)$, which represent the dynamics of large-scale and near-wall

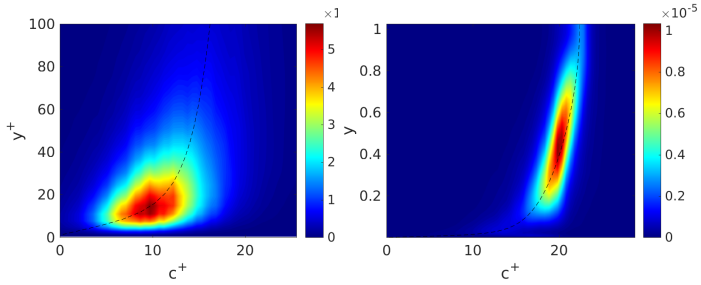

Figure 2: Dependence of the power spectral density $S_{uu}^{(dns)}(\alpha, y, y' = y, \beta, \omega))$ issued from DNS data on the phase speed $c^+ = \omega^+/\alpha^+$ and the wall-normal coordinate for buffer-layer structures with $\lambda_x^+ = 450, \lambda_z^+ = 100$ (left panel) and large-scale structures with $\lambda_x = 3, \lambda_z = 1.5$ (right panel). The mean velocity profile U^+ is reported as a dashed black line. Data from the direct numerical simulation in the LSM flow unit at $Re_\tau = 1007$

self-sustained motions, respectively.

The power cross-spectral density tensor has therefore been computed for the two considered (α, β) pairs. The initial transient of the simulation is discarded and statistics and samples are accumulated starting from $t = 95000$. Welch's method with Hamming windowing and 75% overlap is then used to compute the velocity power cross-spectral density $\mathbf{S}$ using a total of $N_s = 8001$ snapshots of the DNS solutions with sampling interval $(\Delta t)_s = 0.25$ for a total acquisition time $T_{max} = 2000$ for the small scales, and using $N_s = 20001$ snapshots sampled every $(\Delta t)_s = 0.5$ for a total acquisition time $T_{max} = 10000$ for the large scales. The average temporal step of the DNS during the acquisition time is $\overline{\Delta t} = 0.0106$, i.e. $\overline{\Delta t}^+ = 0.35$. Data have also been averaged between the two walls.

The streamwise velocity power spectral density profiles $S_{uu}(\alpha, y, y, \beta, \omega) = \langle \widetilde{u}(\alpha, y, \beta, \omega)\widetilde{u}^*(\alpha, y, \beta, \omega)\rangle$ are reported in Figure (2) as a function of the phase speed $c = \omega/\alpha$, expressed in wall units, and of the wall normal coordinate for the considered (α, β) pairs. The peaks of these distributions are found at $\omega_{max} = 4.3$ and $\omega_{max} = 1.4$ for the near-wall and large-scale peaks, respectively. These peaks correspond to the two phase velocities $c_{max}^+ \approx 10$ and $c_{max}^+ \approx 20$ and their wall-normal locations ($y_{max}^+ \approx 15$ and $y_{max} \approx 0.4 - 0.5$) approximatively correspond to the wall-normal position where $U^+ = c^+$.

4 Estimations from resolvents

The capacity of the ν_t and the ν linear models to reproduce statistics of the turbulent flow via the estimation $\mathbf{S}^{(res)} = p\mathbf{H}\mathbf{H}^*$ given by Eq. (8) is tested by first assuming a (temporal) white noise forcing where $p = \overline{p}$ does not depend on ω and $\overline{p}$ is chosen such that the estimated total spectral power of the streamwise velocity matches the one issued from direct numerical simulations, i.e. $\int_{-\infty}^{\infty}\int_{-1}^{1} {S_{uu}}^{(est)}(\alpha, y, y, \beta, \omega)dyd\omega = \int_{-\infty}^{\infty}\int_{-1}^{1} {S_{uu}}^{(dns)}(\alpha, y, y, \beta, \omega)dyd\omega$. As a second case, colored noise is assumed with $p(\omega)$ such that at each selected frequency ω: $\int_{-1}^{1} {S_{uu}}^{(est)}(\alpha, y, y, \beta, \omega)dy = \int_{-1}^{1} {S_{uu}}^{(dns)}(\alpha, y, y, \beta, \omega)dy$.

The results obtained with the ν-model are reported in Figure (3) where the y-profiles of the estimated streamwise velocity power spectral density versus the phase speed c^+ are shown analogously to Figure (2). For white-

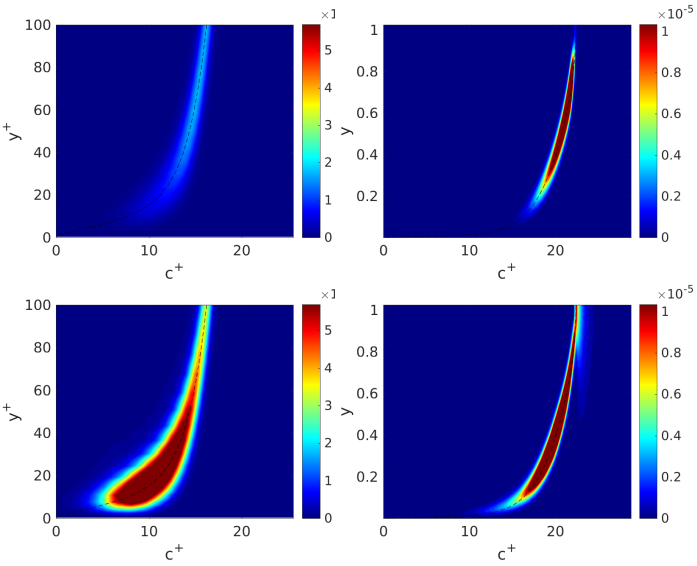

Figure 3: Dependence of $S_{uu}^{(est)}(\alpha, y, y' = y, \beta, \omega))$ estimated with the ν-model on the wall-normal coordinate and the phase speed c^+ with (white-noise) flat-spectrum stochastic forcing (top panels) and coloured-noise stochastic forcing (bottom panels) for the near-wall structures with $\lambda_x^+ = 450, \lambda_z^+ = 100$ (left panels) and the large-scale structures with $\lambda_x = 3, \lambda_z = 1.5$ (right panels). The mean velocity profile U^+ is reported as a dashed black line. The colour-scale is the same as the one used to represent direct numerical simulations data in Figure (2).

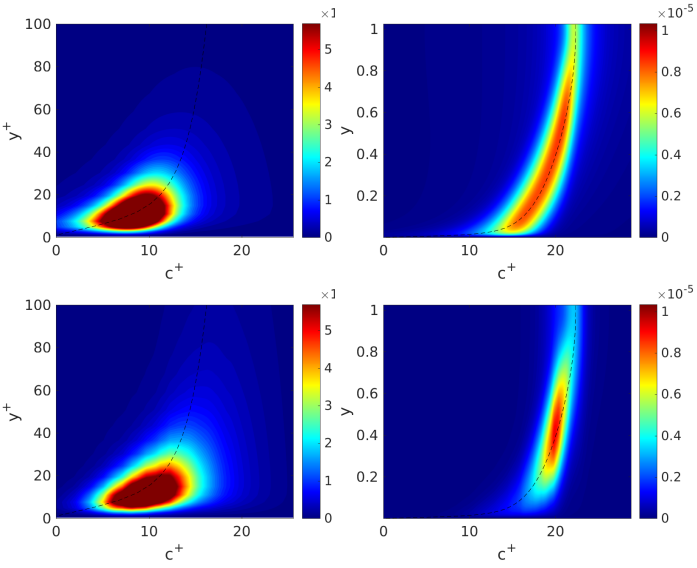

Figure 4: Dependence of $S_{uu}^{(est)}(\alpha, y, y' = y, \beta, \omega))$ estimated with the ν_t-model on the wall-normal coordinate and the phase speed c^+ with (white-noise) flat-spectrum stochastic forcing (top panels) and coloured-noise stochastic forcing (bottom panels) for the near-wall structures with $\lambda_x^+ = 450, \lambda_z^+ = 100$ (left panels) and the large-scale structures with $\lambda_x = 3, \lambda_z = 1.5$ (right panels). The mean velocity profile U^+ is reported as a dashed black line. The colour-scale is the same as the one used to represent direct numerical simulations data in Figure (2)

noise forcing (top panels), the ν-model does not select the correct values and locations of the power spectral density peaks, which are predicted at too large c^+ values (and therefore too large ω values) and are located near the channel center (out of view in the top left panel). The power spectral density appears also to be too narrowly concentrated near the line $U^+ = c^+$ when compared to the DNS data of Figure (2) both for near-wall and large-scale structures. The estimation improves for the case of colored noise (bottom panels), where the selective (in ω) forcing is able to drive the response peaks nearer their DNS values. Even in this case, however, the power spectral density remains too narrowly concentrated and therefore too large near the $U^+ = c^+$ curve (the uniform dark red regions in bottom and right panels which are strongly offscale).

The use of the ν_t model leads to a significant improvement, as shown in Figure (4), of the response near the channel centre because the effective eddy diffusivity dampens (where the eddy viscosity is high) and smoothens the critical layer peaks. The ν_t-model is able to select a reasonable y^+_{max}-c^+_{max} location of the cross-spectral peak for buffer-layer structures even with white-noise stochastic forcing (top panels). For large-scale structures (top right panel), however, the amplitude of the response is still over-predicted near the channel centre and near the wall. The estimation based on the ν_t model is further improved when the coloured-spectrum forcing is used (bottom panels), in particular for the large-scale case (bottom right panel)

5 Conclusions

In this study the 'measured' spatio-temporal power cross-spectral density $\mathbf{S}^{(dns)} = \langle \widetilde{\mathbf{u}}(\alpha, y, \beta, \omega) \widetilde{\mathbf{u}}^*(\alpha, y', \beta, \omega) \rangle$ obtained by direct numerical simulation of plane channel flow at $Re_\tau = 1007$, has been compared to the estimation $\mathbf{S}^{(res)} = p\mathbf{H}\mathbf{H}^*$ based on the resolvent operator $\mathbf{H}$ which implicitly assumes that the spatio-temporal power cross-spectral density of the forcing is of the form $\mathbf{P} = p\,\mathbf{I}$. In this type of analysis the contribution of each temporal frequency ω to the spatial energy spectral density can be analysed separately. The comparison has been performed for structures with spatial scales typical of buffer-layer structures ($\lambda_z^+ = 100, \lambda_x^+ = 450$) and of large-scale motions ($\lambda_z = 1.5, \lambda_x = 3$).

Two distinct linear models have been considered for the evaluation of $\mathbf{H}$, respectively including ('ν_t model') or not (the quasi-laminar model or 'ν model') an eddy viscosity modeling the turbulent Reynolds stresses. Two types of forcing power spectra $p(\omega)$ have been considered: white noise (flat forcing power spectrum $p = \overline{p}$) and 'coloured' noise (power spectrum where $p(\omega)$ is chosen so as to match the power spectrum of the estimated streamwise velocity power spectral density to the measured one).

Qualitatively correct estimations of power cross-spectral density distributions and of the dependence of the power spectral density wall-normal distributions on the frequency (or, equivalently, the phase speed) are found when using the ν_t model resolvent. On the contrary, generally overestimated values of the streamwise velocity power spectral density which are (too) narrowly concentrated near the critical layer are found when using the ν model which is also unable to even qualitatively reproduce the $c^+_{max} - y^+_{max}$ values of the peak amplitude of the power spectral density for buffer-layer structures. It is also found that in all cases, as expected, estimations are improved by using the appropriately coloured input power spectrum $p(\omega)$ instead of white noise as already observed in [26] using a different methodology.

The interpretation of these results is as follows: in the ν model the effect of turbulent Reynolds stresses resides only in the forcing and the associated power cross-spectral density $\mathbf{P}$ while in the ν_t model the effect of turbulent Reynolds stresses is included in the resolvent $\mathbf{H}$. As a consequence, when no accurate information on $\mathbf{P}$ is available, which is the rule at high Reynolds numbers, and it is therefore assumed that $\mathbf{P} = p\mathbf{I}$, the ν_t model performs much better than the ν-model because the effect of the turbulent Reynolds stresses is embedded in $\mathbf{H}$. It is, however, likely that the ν model could perform equally well in the case where a realistic modelling of the forcing cross-spectral tensor $\mathbf{P}$ could be obtained leading to the estimation $\mathbf{S}^{(res)} = \mathbf{H}\mathbf{P}\mathbf{H}^*$. In this second case the scale selection would be dictated by $\mathbf{P}$ instead of $\mathbf{H}$.

The similarity of resolvent modes computed with the ν-model and experimental SPOD modes previously observed in in turbulent jets [17, 27, 18] can be understood by recalling that in free shear-flows the turbulent eddy viscosity usually only weakly depends on the radial coordinate and therefore the resolvent based on the ν-model coincides with the one based on the ν_t-model except for a rescaling by ν/ν_T of the Reynolds number and provided that the solution domain is not too long in the streamwise direction.

Further progress in the estimation of $\mathbf{S}^{(dns)}$ could certainly come from a better modelling of the Reynolds stress tensor in the linear operator and from the modelling of $\mathbf{P}$ related to the regeneration mechanism of the vortices in the self-sustained processes [28, 24, 29, 14]. These research directions are currently actively pursued.

Acknowledgment

Direct numerical simulations were performed on resources provided by the Swedish National Infrastructure for Computing (SNIC) at NSC, HPC2N and PDC

References

[1] W. V. R. Malkus, "Outline of a theory of turbulent shear flow," *J. Fluid Mech.*, vol. 1, pp. 521–539, 1956.

[2] K. M. Butler and B. F. Farrell, "Optimal perturbations and streak spacing in wall-bounded turbulent shear flow.," *Phys. Fluids*, vol. 5, pp. 774–777, 1993.

[3] B. F. Farrell and P. J. Ioannou, "Optimal excitation of three-dimensional perturbations in viscous constant shear flow," *Phys. Fluids*, vol. 5, pp. 1390–1400, 1993.

[4] B. J. McKeon and A. S. Sharma, "A critical-layer framework for turbulent pipe flow," *J. Fluid Mech.*, vol. 658, pp. 336–382, Sept. 2010.

[5] B. J. McKeon, "The engine behind (wall) turbulence: Perspectives on scale interactions," *J. Fluid Mech.*, vol. 817, pp. P1:1–86, Apr. 2017.

[6] W. C. Reynolds and W. G. Tiederman, "Stability of turbulent channel flow, with application to Malkus's theory," *J. Fluid Mech.*, vol. 27, no. 02, pp. 253–272, 1967.

[7] W. C. Reynolds and A. K. M. F. Hussain, "The mechanics of an organized wave in turbulent shear flow. Part 3. Theoretical models and comparisons with experiments," *J. Fluid Mech.*, vol. 54, no. 02, pp. 263–288, 1972.

[8] A. Bottaro, H. Souied, and B. Galletti, "Formation of secondary vortices in a turbulent square-duct flow," *AIAA J.*, vol. 44, pp. 803–811, 2006.

[9] J. C. del Álamo and J. Jiménez, "Linear energy amplification in turbulent channels.," *J. Fluid Mech.*, vol. 559, pp. 205–213, 2006.

[10] C. Cossu, G. Pujals, and S. Depardon, "Optimal transient growth and very large scale structures in turbulent boundary layers," *J. Fluid Mech.*, vol. 619, pp. 79–94, 2009.

[11] G. Pujals, M. García-Villalba, C. Cossu, and S. Depardon, "A note on optimal transient growth in turbulent channel flows," *Phys. Fluids*, vol. 21, p. 015109, 2009.

[12] Y. Hwang and C. Cossu, "Amplification of coherent streaks in the turbulent Couette flow: an input-output analysis at low Reynolds number," *J. Fluid Mech.*, vol. 643, pp. 333–348, 2010.

[13] Y. Hwang and C. Cossu, "Linear non-normal energy amplification of harmonic and stochastic forcing in turbulent channel flow," *J. Fluid Mech.*, vol. 664, pp. 51–73, 2010.

[14] C. Cossu and Y. Hwang, "Self-sustaining processes at all scales in wall-bounded turbulent shear flows," *Phil. Trans. R. Soc. A*, vol. 375, p. 20160088, Mar. 2017.

[15] S. J. Illingworth, J. P. Monty, and I. Marusic, "Estimating large-scale structures in wall turbulence using linear models," *J. Fluid Mech.*, vol. 842, pp. 146–162, May 2018.

[16] C. Picard and J. Delville, "Pressure velocity coupling in a subsonic round jet," *Int. J. Heat Fluid Fl.*, vol. 21, no. 3, pp. 359–364, 2000.

[17] O. Semeraro, V. Jaunet, P. Jordan, A. V. Cavalieri, and L. Lesshafft, "Stochastic and harmonic optimal forcing in subsonic jets," in *22nd AIAA/CEAS Aeroacoustics Conference*, p. 2935, 2016.

[18] A. Towne, O. T. Schmidt, and T. Colonius, "Spectral proper orthogonal decomposition and its relationship to dynamic mode decomposition and resolvent analysis," *J. Fluid Mech.*, vol. 847, pp. 821–867, July 2018.

[19] R. D. Cess, "A survey of the literature on heat transfer in turbulent tube flow," Research Report 8–0529–R24, Westinghouse, 1958.

[20] B. F. Farrell and P. J. Ioannou, "Stochastic forcing of the linearized Navier-Stokes equation," *Phys. Fluids A*, vol. 5, pp. 2600–9, 1993.

[21] J. S. Bendat and A. G. Piersol, *Random data: analysis and measurement procedures.* John Wiley & Sons, 1986.

[22] M. Lee and R. D. Moser, "Direct numerical simulation of turbulent channel flow up to $\mathrm{Re}_\tau \approx 5200$," *J. Fluid Mech.*, vol. 774, pp. 395–415, July 2015.

[23] J. C. del Álamo, J. Jiménez, P. Zandonade, and R. D. Moser, "Scaling of the energy spectra of turbulent channels," *J. Fluid Mech.*, vol. 500, pp. 135–144, 2004.

[24] Y. Hwang and C. Cossu, "Self-sustained process at large scales in turbulent channel flow.," *Phys. Rev. Lett.*, vol. 105, no. 4, p. 044505, 2010.

[25] M. Chevalier, P. Schlatter, A. Lundbladh, and D. S. Henningson, "A Pseudo-Spectral Solver for Incompressible Boundary Layer Flows," Tech. Rep. TRITA-MEK 2007:07, Royal Institute of Technology (KTH), Dept. of Mechanics, Stockholm, 2007.

[26] A. Zare, M. Jovanović, and T. T. Georgiou, "Colour of turbulence," *J. Fluid Mech.*, vol. 812, pp. 636–680, Feb. 2017.

[27] O. T. Schmidt, A. Towne, G. Rigas, T. Colonius, and G. A. Brès, "Spectral analysis of jet turbulence," *J. Fluid Mech.*, vol. 855, pp. 953–982, 2018.

[28] F. Waleffe, "Hydrodynamic stability and turbulence: Beyond transients to a self-sustaining process," *Stud. Appl. Math.*, vol. 95, pp. 319–343, 1995.

[29] Y. Hwang and C. Cossu, "Self-sustained processes in the logarithmic layer of turbulent channel flows," *Phys. Fluids*, vol. 23, p. 061702, 2011.